Vorticity generation in creeping flow past a magnetic obstacle

S. Cuevas*
Centro de Investigación en Energía, UNAM, Apartado Postal 34, Temixco, Morelos 62580, Mexico

S. Smolentsev† and M. Abdou‡
Mechanical & Aerospace Engineering Department, UCLA, 44-114 Engineering IV, Los Angeles, California 90095-1597, USA

(Received 17 February 2006; revised manuscript received 5 September 2006; published 3 November 2006)

The generation of vorticity in the two-dimensional creeping flow of an incompressible, electrically conducting viscous fluid past a localized magnetic field distribution is analyzed under the low magnetic Reynolds number approximation. It is shown that the Lorentz force produced by the interaction of the induced electric currents with the nonuniform magnetic field acts as an obstacle for the flow, creating different steady flow patterns that are reminiscent of those observed in the flow past bluff bodies. First, analytic solutions are obtained for a creeping flow past a magnetic point dipole, modeled as a Gaussian distribution. Using a perturbation scheme, the vorticity is expressed as an expansion in the small Reynolds number, and first- and second-order approximations are calculated. The induced magnetic field, pressure, and stream function are also determined. Further, full numerical finite difference solutions are obtained for a uniform creeping flow past a finite size magnetic field distribution produced by a square magnetized plate. Hartmann numbers in the range $1 \leqslant \mathrm{Ha} \leqslant 100$ are explored. Depending on the strength of the magnetic force, stagnation zones or steady vortical structures are obtained. The analysis contributes to the understanding of flows in nonuniform magnetic fields and flows produced by localized forces.

DOI: 10.1103/PhysRevE.74.056301 PACS number(s): 47.65.−d, 47.15.−x, 47.11.Bc

I. INTRODUCTION

The generation of vortices in fluid systems is interesting because of important applications such as, for instance, those related to mixing and heat transfer enhancement. In tokamak confinement fusion devices, the promotion of vortical flows in liquid-metal blankets may lead to a substantial intensification of heat transfer [1–3]. In fact, the use of solid obstacles as turbulence promoters in magnetohydrodynamic (MHD) flows has been explored by several authors, with the aim of determining the influence of a magnetic field on the vortices generated in the wake behind the obstacle. It has been shown both numerically and experimentally that vortices shed behind a cylinder under a strong uniform magnetic field parallel to the cylinder axis tend to become aligned to the field direction [3–5]. This tendency toward quasi-two-dimensionality is characteristic of MHD flows under strong magnetic fields [6,7].

In general, vorticity can be created by Lorentz forces through the interaction of induced or injected electric currents with applied magnetic fields. Further, the presence of electromagnetic nonuniformities in the flow promotes the creation of internal shear layers that may lead to flow instabilities when inertial effects are non-negligible. That is the case for MHD flow in a duct with a discontinuity in the electrical conductivity of the walls under a uniform magnetic field [2,8]. Inhomogeneities in the applied field can also create vorticity and produce steady or time-dependent flows. However, the understanding of these phenomena is far from complete, since flows in nonuniform magnetic fields have been much less explored than flows in uniform fields. The importance of understanding the nonuniform case is evident, since any real situation will always involve regions where the field is nonuniform. Incidentally, this occurs in many industrial applications (e.g., steel casting). Recently, attention has been given to flows in nonuniform fields [9,10]. In the theoretical study by Alboussière [9] the analogies with geostrophic flows are stressed. This analysis is restricted to duct flows with a magnetic field varying in the axial direction. In turn, Andreev *et al.* [10] performed an experimental study of a liquid-metal flow in a rectangular duct under the influence of an inhomogeneous magnetic field, and identified different flow regions. Their results may serve as a benchmark problem against which numerical simulations can be tested. In the present contribution, a different kind of situation is analyzed, namely, flows that occur under strongly localized magnetic fields. Localized fields produced, for instance, by permanent magnets fixed in the bottom of a container have been used to generate stirring by injecting electric currents in thin fluid layers [11,12]. But stirring can also be created by traveling localized magnetic fields in quiescent fluids or, equivalently, uniform flows past fixed localized fields. Actually, flows of this kind exhibit some features similar to those of ordinary flows around solid obstacles and, as noted in [10], can shed new light on flows in ordinary hydrodynamics. In experiments by Honji [13,14] vortical flows were produced by the interaction of a localized moving magnetic field with an electric current applied through a thin layer of an electrolyte. The experiments were performed using a shallow layer of salt water contained in a long tank, where an electric current was injected transversally to the tank's long axis. A permanent magnet located externally but close to the salt water layer was moved at a constant velocity along the center line of the water tank. Depending on the

*Electronic address: scg@cie.unam.mx
†Electronic address: sergey@fusion.ucla.edu
‡Electronic address: abdou@fusion.ucla.edu

velocity of the magnet and the injected electric current, different flow patterns were generated, including a wavy wake, symmetric vortex pairs, and even periodic vortex shedding. Honji's papers provide valuable experimental evidence, but no theoretical analysis is presented. In turn, Afanasyev and Korabel [15] used a similar device, but performed a much more extensive experimental study in a thin layer of a stratified fluid. They considered flows produced by a single magnet as well as by two magnets with opposite orientations, aligned with the direction of motion and separated by a short distance. For one magnet, they observed the initial formation of vortex dipoles and their subsequent shedding either in the form of a regular Kármán street or an irregular ejection of vortex dipoles. For two magnets, the inverted Kármán vortex street, consisting of interconnected vortex quadrupoles, was observed. It appears that the finite size of the forcing region is a necessary condition for the formation of vortex streets. They approach the problem from the point of view of the hydrodynamic effects of localized forces, since their main interest is the analysis of flows produced by self-propelled bodies (see also [16,17]). However, a magnetohydrodynamic description of the flow is not provided. Recently, the interaction of a uniform flow with a localized magnetic field was analyzed numerically by the authors, considering the case when inertial effects dominate over diffusive ones [18]. Unlike experimental studies, no injected electric currents were considered and Lorentz forces were created instead by the interaction of induced electric currents with a localized field. It was shown that this field acts as an obstacle for the flow and, under certain conditions, an instability leading to vortex shedding can appear. In the present paper, we continue the analysis of the motion of conducting fluids through localized nonuniform fields, but we now restrict ourselves to analyzing the creeping flow regime. It is shown that, even under these conditions, stirring is produced, and different flow patterns can be obtained. For the sake of simplicity, a two-dimensional flow under a localized magnetic field is analyzed. This is justified by experimental evidence that shows the possibility of obtaining quasi-two-dimesional flows in the laboratory [13–15]. First, with the aim of arriving at analytic solutions, we assume that the applied field is produced by an *approximated* magnetic point dipole. This case corresponds to flows produced by point forces, similar to the far-field flow that results in self-propelled bodies when details from the force distribution are not considered [15,16]. In this way, assuming that the flow is slightly perturbed by the Lorentz force, a solution is obtained as an expansion in the small Reynolds number. In the second case, a finite differences numerical solution is obtained when the applied field is produced by a finite square magnetic dipole for which an analytic expresion is available. The strength and finite size area of the magnetic field distribution introduce important electromagnetic effects that lead to different flow structures.

II. FORMULATION

We consider a two-dimensional flow of an electrically conducting incompressible viscous fluid in an unbounded region where a nonuniform magnetic field produced by a localized source is present. Far from the source, the fluid displays a uniform flow of magnitude U in the positive x direction. We will consider that the magnetic source is of dipolar nature although different distributions can also be considered. The motion of the fluid within the applied field induces electric currents which generate an induced field $\mathbf{b}$, so that the total magnetic field is given by $\mathbf{B}=\mathbf{B}^0+\mathbf{b}$. The induced electric currents interact with $\mathbf{B}^0$, giving rise to a nonuniform Lorentz force that modifies the original flow and creates vorticity. We assume that the induced field is much smaller than the applied field, $\mathbf{b}\ll\mathbf{B}^0$, which means that the magnetic Reynolds number $\mathrm{Rm}=\mu\sigma UL$ is much less than unity. Here, μ and σ are the magnetic permeability and the electrical conductivity of the fluid, respectively, and L is a characteristic length to be defined below. This condition is satisfied in most laboratory and industrial flows with liquid metals, molten salts, and electrolytes. We also assume that the flow is confined to the xy plane and that the magnetic moment of the dipole source points in the direction normal to the plane of flow (see Fig. 1). Therefore, the dominant contribution of the applied field comes from the normal component (in the positive z direction) and is the only one considered (i.e., a straight magnetic field approximation [9]). Under these conditions, induced currents will form loops in the plane of motion so that the induced magnetic field $\mathbf{b}$ points also in the z direction. In turn, components of the Lorentz force will appear in the plane of flow. Actually, the Lorentz force will be negligible everywhere except in the neighborhood of the magnetic dipole. The dimensionless equations of motion take the form

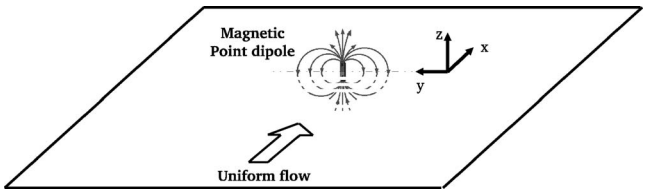

FIG. 1. Sketch of the two-dimensional problem considered.

$$\frac{\partial u}{\partial x}+\frac{\partial v}{\partial y}=0, \tag{1}$$

$$\frac{\partial u}{\partial t}+\mathrm{Re}\left(u\frac{\partial u}{\partial x}+v\frac{\partial u}{\partial y}\right)=-\frac{\partial p}{\partial x}+\nabla_\perp^2 u+(\mathrm{Ha})^2 j_y B_z^0, \tag{2}$$

$$\frac{\partial v}{\partial t}+\mathrm{Re}\left(u\frac{\partial v}{\partial x}+v\frac{\partial v}{\partial y}\right)=-\frac{\partial p}{\partial y}+\nabla_\perp^2 v-(\mathrm{Ha})^2 j_x B_z^0, \tag{3}$$

where the subindex $\perp$ denotes the projection of the ∇ operator on the xy plane. Here, the velocity components u and v are normalized by U; the pressure p by $\rho\nu U/L$; the electric current density components j_x and j_y by σUB_m; and the applied field B_z^0 by B_m, where B_m is a characteristic strength of the magnetic dipole to be defined below. The dimensionless coordinates x and y are normalized by L, while time t is normalized by the viscous time L^2/ν. This normalization is commonly used in creeping flow problems. The dimensionless parameter $\mathrm{Ha}=B_mL\sqrt{\sigma/\rho\nu}$ is the Hartmann number,

whose square can be interpreted as the ratio of magnetic to viscous forces, where ρ and ν are the mass density and the kinematic viscosity of the fluid, respectively. In turn, $\mathrm{Re}=UL/\nu$ is the Reynolds number, which denotes the ratio of inertia and viscous forces.

The Maxwell equations in the quasistatic approximation can be combined to give the induction equation. In the two-dimensional case, neglecting $O(\mathrm{Rm})$ terms, this equation reduces to a single equation for the component b_z [18], namely,

$$\nabla_\perp^2 b_z - u\frac{\partial B_z^0}{\partial x} - v\frac{\partial B_z^0}{\partial y} = 0, \tag{4}$$

where the induced magnetic field b_z has been normalized by $\mathrm{Rm}\, B_m$. Since b_z is independent of the z coordinate, the condition $\nabla\cdot\mathbf{b}=0$ is satisfied. Once $\mathbf{b}$ is determined, Ampere's law $\nabla\times\mathbf{b}=\mathbf{j}$ gives an expression to calculate electric currents. This equation also guarantees that the electric current density is divergence-free, $\nabla\cdot\mathbf{j}=0$. Hence, the current density components are given by

$$j_x = \frac{\partial b_z}{\partial y}, \quad j_y = -\frac{\partial b_z}{\partial x}. \tag{5}$$

Equations (5) show that the induced magnetic field serves as a stream function for the electric current in the plane of flow. Therefore, lines of $b_z=\mathrm{const}$ are current streamlines.

A. Boundary conditions

We assume that far away from the magnetic dipole, a steady uniform flow in the positive x direction is imposed. With the origin of coordinates located at the point of maximum magnetic field strength, the boundary conditions on the velocity components are

$$u \to 1, \quad v \to 0 \quad \text{as } x,y \to \pm\infty. \tag{6}$$

It is obviously expected that the strength of the induced magnetic field is higher near the zone where the applied magnetic field is strong. As the distance from the source of the applied field grows, the induced field must decrease and vanish at infinity. Therefore, it must satisfy

$$b_z \to 0 \quad \text{as } x,y \to \pm\infty. \tag{7}$$

We now look for analytic solutions of these equations in a simplified case.

III. CREEPING FLOW PAST A MAGNETIC POINT DIPOLE

In order to carry out an approximate analytic approach, we analyze the generation of vorticity when a creeping flow interacts with a magnetic point dipole. The three-dimensional expression of the magnetic field produced by a point dipole is given, for instance, in the book by Good and Nelson [19]. Here we disregard the dependence on the z coordinate; therefore, the dimensional normal component of a *two-dimensional* point dipole located at the origin with its magnetic dipole moment pointing in the positive z direction is given by

$$\mathcal{B}_z^0 = \frac{\mu m}{2\pi}\frac{1}{X^2+Y^2} + \mu m\,\delta(X)\,\delta(Y), \tag{8}$$

where $\mathcal{B}_z^0$ stands for the dimensional magnetic field, m is the magnitude of the magnetic dipole moment, and X and Y are the dimensional coordinates. The first term on the right-hand side of Eq. (8) gives the field outside the source, that is, at any position except the origin, while the second term accounts for the effect of the singularity through the Dirac δ functions [19]. The field $\mathcal{B}_z^0$ can be normalized by $B_m=\mu m/L^2$, where the characteristic length L has to be specified. For a finite size dipole, the length L can be chosen without ambiguity, however, there is no natural characteristic length for a point dipole. For practical purposes we choose L in such a way the normalization constant $\mu m/L^2$ takes a value of 1, that is, $L=\sqrt{\mu m}$.

In order to linearize the equations of motion, we assume that the flow past the magnetic point dipole is only slightly perturbed by the Lorentz force produced by the interaction of the induced electric currents with the applied field. Therefore, the dimensionless velocity components can be expressed as

$$u = 1 + u', \quad v = v', \tag{9}$$

where u' and v' are the perturbations in the oncoming uniform flow due to the presence of the magnetic dipole. Assuming that $u', v' \ll 1$, and neglecting products of the derivatives of the field with u' and v', the magnetic induction equation (4) reduces to

$$\nabla_\perp^2 b_z = \frac{\partial B_z^0}{\partial x}, \tag{10}$$

where B_z^0 is given by Eq. (8) normalized by B_m. Notice that this equation is uncoupled from the velocity perturbations. In this approximation the induced field b_z is generated by a uniform unperturbed flow. Let us now consider the associated time-dependent problem, namely,

$$\frac{\partial b_z}{\partial t'} = \nabla_\perp^2 b_z - \frac{\partial B_z^0}{\partial x}. \tag{11}$$

The solution of Eq. (11) that satisfies boundary condition (7) in the infinite domain $-\infty<x<\infty$, $-\infty<y<\infty$ for $t'>0$, can be obtained by the Green's function method with the initial condition $b_z=0$ for $t'=0$ (see Ref. [12]). In fact, only the term with the Dirac delta function in Eq. (8) gives a nonzero contribution to the induced field. The result is

$$b_z(x,y,t') = \frac{1}{2\pi}\frac{x}{x^2+y^2}e^{-(x^2+y^2)/4t'}, \tag{12}$$

which in the limit $t'\to\infty$ reduces to the steady field

$$b_z(x,y) = \frac{1}{2\pi}\frac{x}{x^2+y^2}. \tag{13}$$

Due to the nature of the applied magnetic field source, solution (13) diverges at the origin. Figure 2(a) shows the isolines of the induced magnetic field given by Eq. (13), while Fig. 2(b) presents the variation of b_z with respect to the

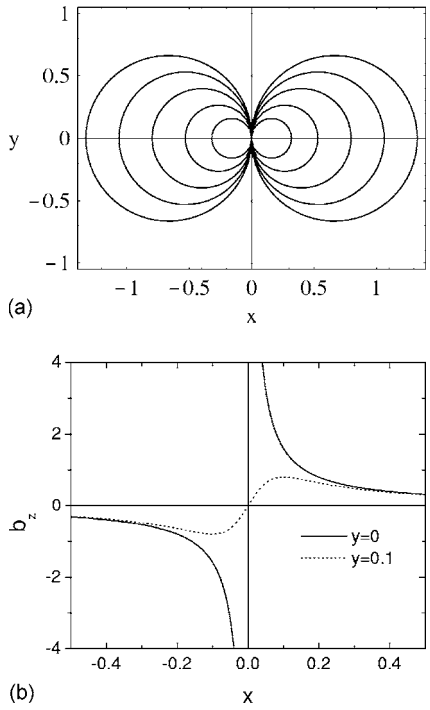

FIG. 2. (a) Isolines of induced magnetic field in creeping flow past a magnetic point dipole. (b) Induced field as a function of the axial coordinate at $y=0$ and $y=0.1$.

streamwise coordinate. This reveals that the flow past the magnetic point dipole generates two symmetric current loops, upstream and downstream of the location of the obstacle, with clockwise and counterclockwise circulation, respectively. Hence, in the neighborhood of the origin, the flow of current in the negative direction is intensified. Due to the direction of the applied field, this produces a localized Lorentz force that opposes the fluid motion and causes an abrupt change in the pressure in the neighborhood of the point dipole.

A. First-order solution

The perturbation to the flow field can be found through the solution of Eqs. (1)–(3). By introducing Eq. (9) into (1)–(3) and neglecting second-order products in the perturbed velocities, a linearized system of equations is obtained. Taking the curl, we get a transport equation for the only vorticity component, $\omega_z=\partial v'/\partial x-\partial u'/\partial y$, namely,

$$\frac{\partial \omega_z}{\partial t}+\mathrm{Re}\frac{\partial \omega_z}{\partial x}=\nabla_\perp^2\omega_z+(\mathrm{Ha})^2\left(\frac{\partial(j_xB_z^0)}{\partial x}+\frac{\partial(j_yB_z^0)}{\partial y}\right). \tag{14}$$

Note that the convective term $\mathrm{Re}\,\partial\omega_z/\partial x$ is similar to the Oseen term in the flow past a solid obstacle. We now look for steady state solutions by expanding the vorticity in terms of the small parameter Re, that is,

$$\omega_z=\omega_z^{(0)}+\mathrm{Re}\,\omega_z^{(1)}+O(\mathrm{Re}^2). \tag{15}$$

Therefore, at $O(\mathrm{Re}^0)$ the vorticity satisfies the equation

$$\nabla_\perp^2\omega_z^{(0)}=(\mathrm{Ha})^2\left(j_x\frac{\partial B_z^0}{\partial x}+j_y\frac{\partial B_z^0}{\partial y}\right), \tag{16}$$

where conservation of current has been used. The right-hand side of Eq. (16) is known at the leading order of approximation, since the current density components can be calculated explicitly from Eqs. (5) and (13). Here, with the aim of arriving at simple analytical solutions, instead of Eq. (8), the normal component of the applied magnetic field is approximated through the Gaussian distribution

$$B_z^0(x,y)=\frac{n}{\pi}e^{-n(x^2+y^2)},\quad n>0. \tag{17}$$

Equation (17) is a good approximation of the product of Dirac δ functions in the second term of Eq. (8), namely, the term that contributes to the induced field. In fact, both expressions present similar distributions arround the origin when $n\gg 1$. Also, the integral of Eq. (17) in the infinite domain is equal to 1, as occurs with the second term of Eq. (8). Using this expression, Eq. (16) can be written in cylindrical coordinates in the form

$$\frac{1}{r}\frac{\partial}{\partial r}\left(r\frac{\partial\omega_z^{(0)}}{\partial r}\right)+\frac{1}{r^2}\frac{\partial^2\omega_z^{(0)}}{\partial\theta^2}=(\mathrm{Ha})^2\left(\frac{n}{\pi}\right)^2\frac{e^{-nr^2}}{r}\sin\theta. \tag{18}$$

The solution of this equation is

$$\omega_z^{(0)}(r,\theta)=\left[\frac{C_1}{r}+C_2r-\frac{n(\mathrm{Ha})^2}{4\pi^2}\left(\frac{e^{-nr^2}}{r}+nr\mathrm{Ei}(-nr^2)\right)\right]\sin\theta, \tag{19}$$

where

$$\mathrm{Ei}(z)=-\int_{-z}^{\infty}\frac{e^{-t}}{t}dt\quad\text{for } z>0.$$

From Eqs. (6), the condition $\omega_z\to 0$ as $r\to\infty$ must be satisfied, therefore, $C_2=0$. To avoid further divergence at $r=0$, the constant C_1 is set equal to zero. In Cartesian coordinates we have

$$\omega_z^{(0)}(x,y)=-\frac{n(\mathrm{Ha})^2}{4\pi^2}\left(\frac{ye^{-n(x^2+y^2)}}{x^2+y^2}+ny\mathrm{Ei}[-n(x^2+y^2)]\right). \tag{20}$$

Note that ω_z^0 and, consequently, the velocity perturbations u' and v', are $O((\mathrm{Ha})^2)$. Therefore, the assumption $u',v'\ll 1$ limits the solution to small values of the Hartmann number. However, even at small Hartmann numbers the generation of vorticity is clearly manifested, as can be observed in Figs. 3(a) and 3(b), where the solution (20) is plotted for $Ha=0.1$ and $n=100$. Figure 3(a) shows the vorticity isolines, while Fig. 3(b) presents the vorticity as a function of the streamwise coordinate at different cross-stream positions. These figures show that symmetric regions of positive and negative vorticity are created due to the presence of the point dipole. The symmetry observed in the solution shows the lack of convective effects and the dominance of diffusion.

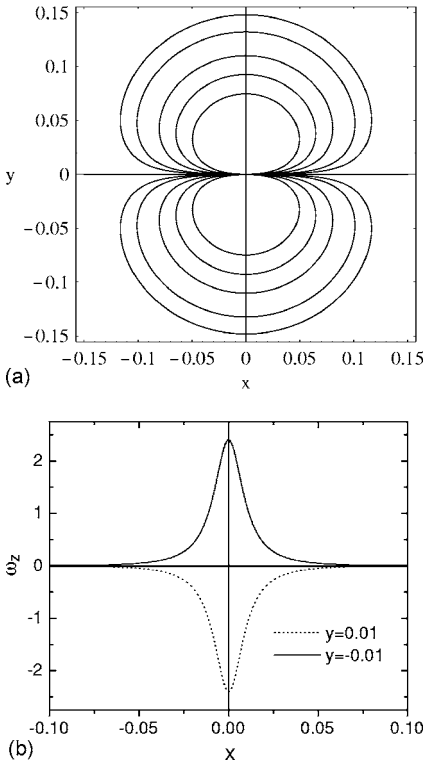

FIG. 3. (a) Vorticity isolines at $O(1)$ in the flow past a magnetic point dipole. (b) Vorticity as a function of the axial coordinate at $y=\pm 0.01$. Ha=0.1, $n=100$.

Once the vorticity is known, the stream function ψ can be determined by solving the equation $\nabla_\perp^2 \psi = -\omega_z$. Expanding the stream function in the form

$$\psi = \psi^{(0)} + \mathrm{Re}\,\psi^{(1)} + O(\mathrm{Re}^2), \tag{21}$$

we get, at first order,

$$\nabla_\perp^2 \psi^{(0)} = -\omega_z^{(0)}. \tag{22}$$

The solution of this equation that satisfies the condition of a uniform flow at infinity, namely, $\partial\psi^{(0)}/\partial y \to 1$ as $x, y \to \infty$, is

$$\psi^{(0)}(x,y) = y - \frac{(\mathrm{Ha})^2}{32\pi^2}\left[(1+n(x^2+y^2))\frac{y}{x^2+y^2}e^{-n(x^2+y^2)} + ny[2+n(x^2+y^2)]\mathrm{Ei}[-n(x^2+y^2)]\right]. \tag{23}$$

Figure 4 shows the streamlines given from Eq. (23) for the case Ha=0.1 and $n=100$. Recirculation zones are formed up- and downstream from the point dipole, causing the deflection of the oncoming flow. The similarities with the flow past solid obstacles, in particular with the flow past a cylinder, are close.

The equation for the pressure can be obtained by taking the divergence of the equations of motion (2) and (3), namely,

$$\nabla_\perp^2 p = (\mathrm{Ha})^2\left(\frac{\partial(j_y B_z^0)}{\partial x} - \frac{\partial(j_x B_z^0)}{\partial y}\right), \tag{24}$$

or, explicitly,

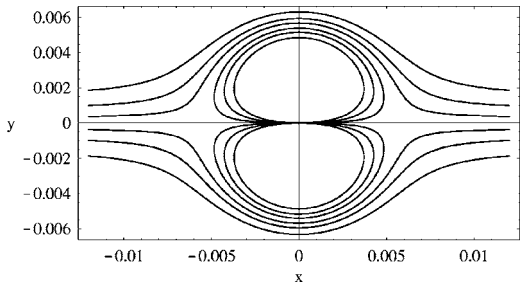

FIG. 4. Stream function at $O(1)$ in creeping flow past a magnetic point dipole. Ha=0.1, $n=100$.

$$\nabla_\perp^2 p = (\mathrm{Ha})^2\left(\frac{n}{\pi}\right)^2 \frac{x}{x^2+y^2}e^{-n(x^2+y^2)}. \tag{25}$$

The solution of Eq. (25) that satisfies the condition of a constant pressure gradient at infinity, namely, $\partial p/\partial x = G = \mathrm{const}$ as $x, y \to \infty$, is the following:

$$p(x,y) = -\frac{n}{\pi^2}\frac{(\mathrm{Ha})^2}{4}\left(\frac{xe^{-n(x^2+y^2)}}{x^2+y^2} + nx\mathrm{Ei}[-n(x^2+y^2)]\right) + Gx. \tag{26}$$

Solution (26) is plotted in Fig. 5 for Ha=0.1, $n=100$. It shows the variation of the pressure with the axial coordinate at two dfferent cross-stream positions. Notice the abrupt change in the pressure as the flow crosses the point dipole; the steep pressure rise and drop is produced by the Lorentz force created in the neighborhood of the dipole.

B. Second-order solution

At $O(\mathrm{Re})$, the vorticity satisfies the equation

$$\nabla^2 \omega_z^{(1)} = \frac{\partial \omega_z^{(0)}}{\partial x},$$

or explicitly

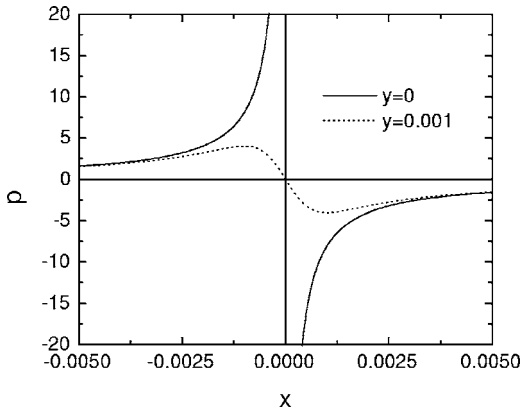

FIG. 5. Pressure as a function of the axial coordinate at $y=0$ and $y=0.001$. Ha=0.1, $n=100$, $G=-1$.

$$\nabla^2 \omega_z^{(1)} = -\frac{n(\mathrm{Ha})^2}{2\pi^2} \frac{x}{(x^2+y^2)^2} e^{-n(x^2+y^2)}. \tag{27}$$

The solution of Eq. (27) that satisfies the condition $\omega_z^{(1)} \to 0$ as $x, y \to \infty$ is

$$\omega_z^{(1)} = \frac{(\mathrm{Ha})^2}{16\pi^2} \left([-1 + n(x^2+y^2)] \frac{xy}{(x^2+y^2)^2} e^{-n(x^2+y^2)} + n^2 xy \mathrm{Ei}[-n(x^2+y^2)] \right). \tag{28}$$

Note that this solution is not symmetric with respect to the yz plane. This is due to the effect of the slight convection introduced in the flow. To this order, a parallel can be made with the solution given by the Oseen approximation in the flow past a bluff body.

The stream function at $O(\mathrm{Re})$ can be determined by solving the equation

$$\nabla_\perp^2 \psi^{(1)} = -\omega_z^{(1)}, \tag{29}$$

which has to satisfy the condition $\partial \psi^{(1)} / \partial y \to 0$ as $x, y \to \infty$. The solution is

$$\psi^{(1)} = \frac{(\mathrm{Ha})^2}{192 n \pi^2} \left(\{-1 + n(x^2+y^2)[2 + n(x^2+y^2)]\} \times \frac{xy}{(x^2+y^2)^2} e^{-n(x^2+y^2)} + n^2 xy[3 + n(x^2+y^2)] \times \mathrm{Ei}[-n(x^2+y^2)] \right). \tag{30}$$

For $\mathrm{Re} \ll 1$, the corrections provided by Eqs. (28) and (30) to the vorticity and stream function, respectively, only modify slightly the results given by the first-order solutions. It is important to stress that all the analytic solutions obtained in this section diverge at the origin. This behavior can be explained by the fact that the source of the applied magnetic field, that is, the magnetic point dipole, presents a singularity at the origin. However, solutions present the correct behavior as the distance from the dipole tends to infinity. Although these solutions are limited to small values of both Re and Ha, the effects of the magnetic point dipole on the flow are shown in a simple manner. This approach is a useful independent check, within the corresponding limits, of the results obtained with the finite difference numerical method presented in the next section.

IV. CREEPING FLOW PAST A FINITE MAGNETIC DIPOLE

We now consider the creeping flow past a magnetic field produced by a square magnetized plate uniformly polarized in the normal direction for which an analytic expression is available. In dimensional terms, placing the coordinate system in the center of a rectangular surface with side lengths $X_0 = 2a$ and $Y_0 = 2b$, the normal component of the field produced by a single magnetized surface lying on the plane $Z = Z_0$ is given by [20]

$$\mathcal{B}_z^0 = \gamma B_{max} \left[\tan^{-1}\left(\frac{(X+a)(Y+b)}{(Z-Z_0)[(X+a)^2+(Y+b)^2+(Z-Z_0)^2]^{1/2}} \right) + \tan^{-1}\left(\frac{(X-a)(Y-b)}{(Z-Z_0)[(X-a)^2+(Y-b)^2+(Z-Z_0)^2]^{1/2}} \right) - \tan^{-1}\left(\frac{(X+a)(Y-b)}{(Z-Z_0)[(X+a)^2+(Y-b)^2+(Z-Z_0)^2]^{1/2}} \right) - \tan^{-1}\left(\frac{(X-a)(Y+b)}{(Z-Z_0)[(X-a)^2+(Y+b)^2+(Z-Z_0)^2]^{1/2}} \right) \right], \tag{31}$$

where $\mathcal{B}_z^0$ stands for the dimensional applied magnetic field, B_{max} is the maximum magnetic field strength, and γ is a normalization constant. This expression gives the normal component of the magnetic field generated by a finite size dipole. For the sake of simplicity, we consider that the magnetized surface has a square shape, that is, $2a = 2b = L$. Therefore, in this case, this length is taken as the geometrical length scale used to nondimensionalize the flow variables while $B_m = B_{max}$. In addition, we consider that the surface is separated from the plane of motion by a distance L, being located at $Z = -L$.

A. Numerical implementation

Analytic solutions for the flow past the magnetic field given by Eq. (31) are very difficult to obtain. Therefore, we look for numerical solutions using a formulation based on the primitive variables, the velocity and pressure, and the induced magnetic field as electromagnetic variable. A finite difference method on an orthogonal equidistant grid was used to solve the governing Eqs. (1)–(4) under suitable boundary conditions, assuming a motionless fluid as initial condition. The standard time-marching procedure described in [21] was extended to consider MHD flows. The numerical method is discussed in more detail in [18].

The numerical solution was obtained in a rectangular domain with a length of 30 units (measured in terms of the characteristic length L) in the streamwise direction and 20 units ($H = 20$) in the cross-stream direction. A suitable location of the magnetic obstacle was determined so that inlet effects as well as upstream effects from the outlet could be minimized. Since for low Reynolds numbers the transport of

vorticity is mainly diffusive, the center of the magnetic obstacle, that is, the point of maximum magnetic field strength, was placed in the geometrical center of the integration region. It was determined that this location guaranteed results that are nearly independent of the position of the obstacle. In turn, the separation H between the lateral boundaries determines the solid blockage of the confined flow characterized by the blockage parameter $\beta=1/H$, which in this case was fixed at 5%. A distribution of six and ten nodes over one unit length in the streamwise and cross-stream directions, respectively, was used with a 211×201 grid.

Boundary conditions (6) and (7) were adapted to the numerical implementation. A uniform flow in the x direction was prescribed at the inlet, namely,

$$u=1, \quad v=0. \tag{32}$$

At the outlet, Neumann conditions were used:

$$\frac{\partial u}{\partial x}=\frac{\partial v}{\partial x}=0. \tag{33}$$

At the lateral boundaries, symmetry-type conditions simulating a frictionless wall were imposed, namely,

$$\frac{\partial u}{\partial y}=v=0. \tag{34}$$

Finally, we assume that the induced field is zero at a long enough finite distance from the source of the applied field. Therefore, we impose that the single component of the induced field satisfies the condition

$$b_z|_S=0, \tag{35}$$

where the subindex S denotes all the boundaries of the integration domain.

B. Numerical results

We explored the flow for a Reynolds number of 0.05 while the Hartmann number varied in the range $1\leqslant \mathrm{Ha} \leqslant 100$. (Reynolds numbers 100 and 200 were explored in [18].) Under these conditions, a balance is established among pressure, and the Lorentz and viscous forces and the flow displays only steady laminar solutions.

Due to the similarities with the flow around bluff bodies, we used the base pressure coefficient to characterize the flow past a magnetic obstacle. The hydrodynamic base pressure coefficient is defined as [22]

$$C_{pb}=1+\frac{p_{180}-p_0}{p_d}, \tag{36}$$

where p_0 and p_{180} are the pressures at the furthest upstream and downstream points on the body surface, and p_d is the free stream dynamic pressure $\rho U^2/2$. Since in our problem there is no solid obstacle, we consider p_0 and p_{180} to be the pressures on the axial midline at the furthest upstream and downstream points, respectively, on the perimeter of the projection of the magnetized surface on the plane of motion. We found that C_{pb} or its negative [known as the base suction coefficient $(-C_{pb})$], are suitable quantities for the description

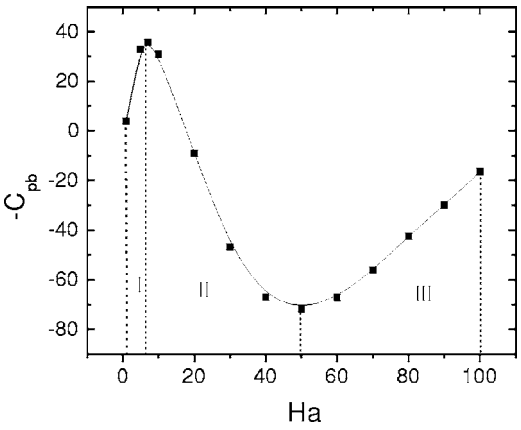

FIG. 6. Base suction coefficient as a function of the Hartmann number for Re=0.05.

of the present problem. Williamson [23] emphasized that the base suction coefficient is particularly useful as a basis for discussion of the various flow regimes. Figure 6 shows the calculated base suction coefficient versus the Hartmann number for Re=0.05. Three different steady flow regimes can be identified as Ha is increased within the explored range. The transition from one regime to the other is featured by a sign change in the slope of the curve. The behavior of this coefficient as Ha grows can be explained by the current density distribution in the obstacle region. For small Hartmann numbers, only two current loops exist, and the Lorentz force opposes the main flow everywhere. As Ha grows, inner current loops appear inside the obstacle, and the Lorentz force opposes the flow at the entrance of the obstacle, while it may act in favor of or against the flow at the obstacle exit, altering the pressure distribution. All regimes show quasisymmetric patterns of vorticity that extend mainly toward the lateral fringing zones. Thick shear layers are displaced by the obstacle forming symmetric sidewise regions, the extension of which is strongly affected by the blockage effect, as occurs in the flow around a cylinder [24]. The diffusive transport of vorticity embraces a substantial portion of the flow domain up- and downstream of the center of the obstacle.

C. Regime I: $1\leqslant \mathrm{Ha} \leqslant 7$

In this regime, the flow passes through the region of maximum magnetic field intensity, presenting only a slight deviation from the main streamwise direction. Figure 7 shows results for Ha=1 which are typical for this regime. The induced field, displaying two symmetric loops, is shown in Fig. 7(a). The projection of the magnetized surface on the plane of motion is shown through a unit square (centered at $x=15$, $y=10$) for visualization purposes. Notice the strong similarity with the analytic solution shown in Fig. 2(a). Since with a finite size magnetic dipole, singularities disappear, the induced field takes negative values upstream of the obstacle and smoothly changes to positive values as it goes downstream. Inside the obstacle, the current is distributed uniformly and directed in the negative y direction; therefore, the Lorentz force opposes the fluid motion in this region. The abrupt rise and fall of the pressure originated by the Lorentz

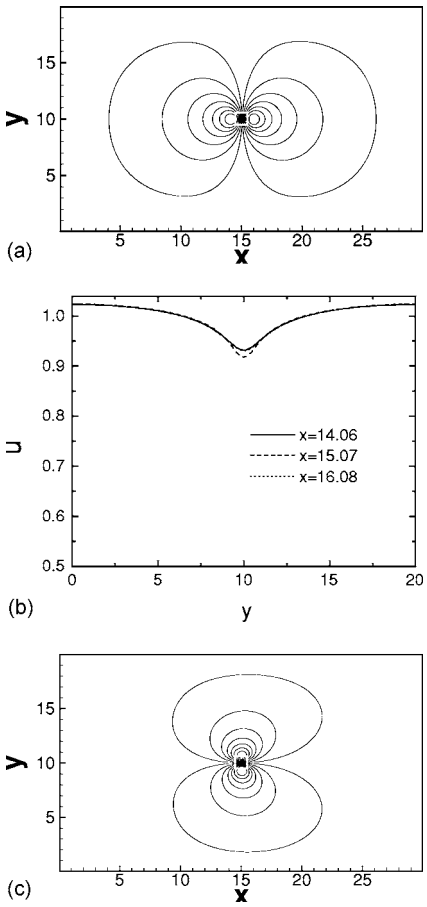

FIG. 7. Regime I. (a) Isolines of induced magnetic field. (b) Streamwise velocity component vs cross-stream coordinate. (c) Isolines of vorticity. Re=0.05, Ha=1.

force takes place continuously in a distance on the order of the characteristic length. The opposing Lorentz force causes a deficit of less than 10% in the streamwise velocity [see Fig. 7(b)] and the appearance of a small cross-stream component two orders of magnitude smaller than the streamwise velocity. The occurrence of a vertical velocity component in the obstacle region gives rise to a local shear flow that is more pronounced the higher the Hartmann number. Figure 7(c) shows the vorticity isolines. Vorticity is concentrated in the neighborhood of the obstacle, displaying positive and negative values in the lower and upper zones, respectively, with a quite symmetric distribution. Again, notice the similarities with Fig. 3(a). A retarded flow region upstream the obstacle and a wake are formed, extending as far as eight and ten units, respectively, at the centerline, where vorticity falls to 1% of its maximum value. The symmetry observed in the flow and induced magnetic field distributions shows the negligible effect of convection.

D. Regime II: $7 < Ha < 50$

The second regime is characterized by the appearance of two small loops of induced magnetic field (i.e., closed electric current paths) inside the region of the obstacle, in addition to the pair of external loops also observed in the

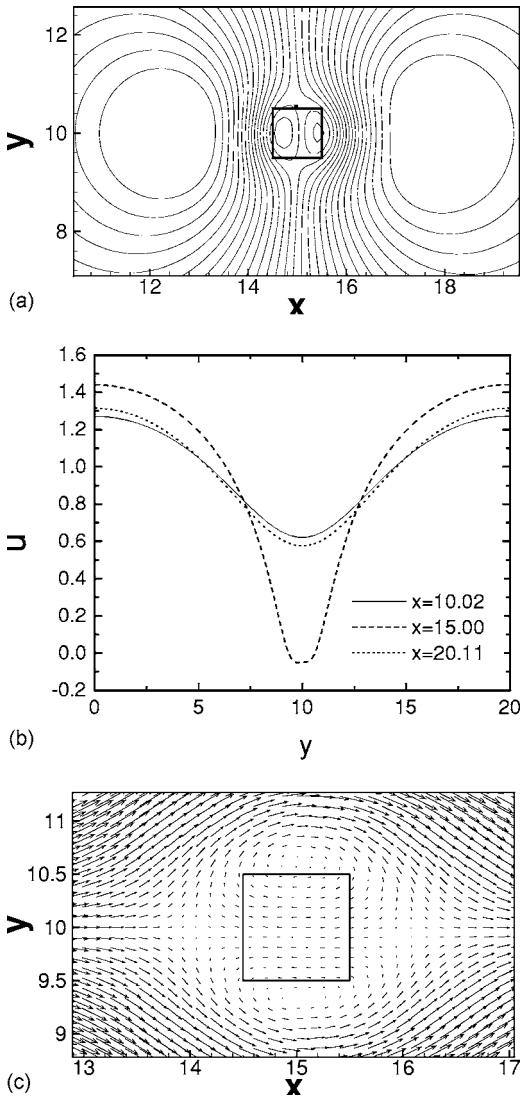

FIG. 8. Regime II. (a) Isolines of induced magnetic field. (b) Streamwise velocity component vs cross-stream coordinate. (c) Velocity field near the obstacle zone. Re=0.05, Ha=30.

previous regime. In Fig. 8(a), isolines of induced magnetic field are shown for the case Ha=30. The existence of inner current loops modifies the flow dynamics in a noticeable way. The pressure drop in the neighborhood of the obstacle does not present a smooth transition as in the previous regime, and the deficit of velocity in the streamwise direction in this region is more than 100%, presenting negative velocities inside the obstacle [see Fig. 8(b)]. Vorticity patterns are very similar to those observed in regime I. Due to the stronger Lorentz force opposing the flow in the upstream fringing region, the fluid circulates around the obstacle, increasing the cross-stream velocity components to reach the same order of magnitude as the streamwise components and intensifying the shear layers formed in the lateral fringing regions. As a consequence, two tenuous recirculation zones (counter-rotating vortices) are formed [see Fig. 8(c)]. The upper and lower vortices present a clockwise and counterclockwise circulation, respectively. Velocity components in the central region are of the order 10^{-3}. Unlike the separated shear layers

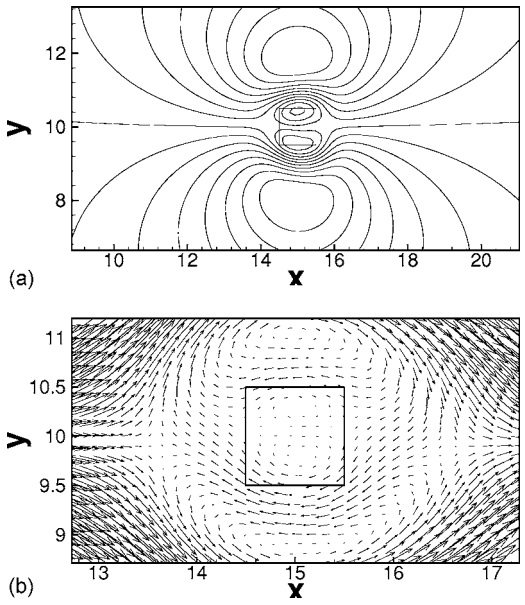

FIG. 9. Regime III. (a) Isolines of vorticity. (b) Velocity field near the obstacle zone. Re=0.05, Ha=70.

that form symmetric steady vortices in the near wake of a cylinder, in this case, vortices appear inside the obstacle. The vortices grow as Ha increases, and they can extend beyond the fringing zones.

E. Regime III: 50≤Ha≤100

In the third regime, the inner current loops persist, but they are increasingly distorted the larger the Hartmann number. As Ha is increased, the flow zone that is substantially affected by the magnetic obstacle grows to about three times the size of the magnetized plates. In Fig. 9 the vorticity isolines [Fig. 9(a)] and the velocity field in the neighborhood of the magnetic obstacle [Fig. 9(b)] are shown for Ha=70. The Lorentz force opposing the flow upstream causes its deviation from the streamwise direction within a distance of about two units from the point of maximum magnetic field strength [see Fig. 9(b)]. The fluid flows around the obstacle, creating a very small velocity region in its interior $[O(10^{-4})]$ characterized by four recirculation zones. In fact, the pair of vortices that originally appeared in regime II are expelled to the lateral fringing zones while a new pair of small counter-rotating vortices appear in the central region.

At the extremes of the steady symmetric vortices that appear inside the obstacle region in regimes II and III, stagnation points can be identified. The location of these points depends on the Hartmann number and their separation gives an estimate of the size of the vortices or, in some sense, of the size of the obstacle. Figure 10(a) shows the distance L_S, between the upstream and downstream stagnation points as a function of the Hartmann number. For Ha$<$50, the stagnation point lies on the axial centerline; however, it is slightly displaced in the negative y direction as Ha grows. It can be observed that, for Ha$\geqslant$20, L_S grows linearly with Ha and approximately satisfies the relation L_S=0.02Ha. Also, the width of the vortices as Ha increases is about the same as

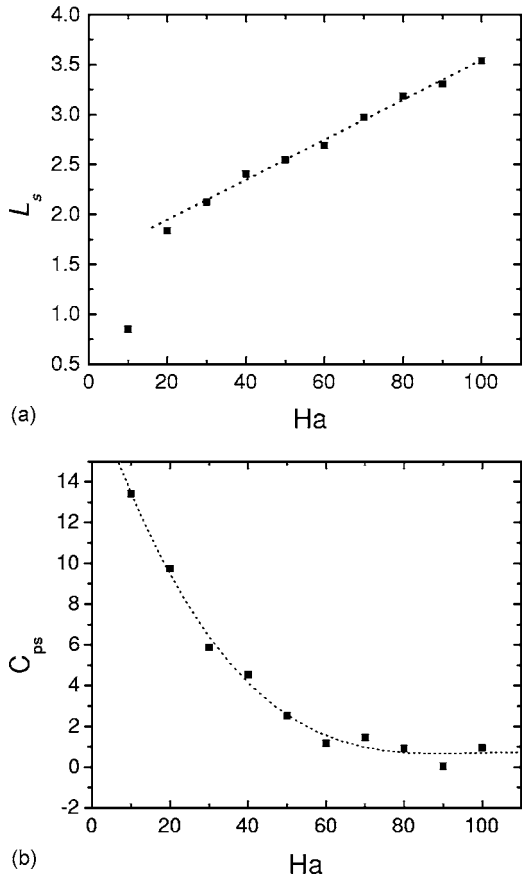

FIG. 10. (a) Distance between stagnation points as a function of the Hartmann number. (b) Stagnation pressure coefficient as a function of the Hartmann number. Re=0.05.

their elongation. Therefore, the size of the vortices grows as $(\mathrm{Ha})^2$.

A stagnation pressure coefficient can also be defined in the following form:

$$C_{ps} = \frac{p_s - p_\infty}{p_d}, \tag{37}$$

where p_s is the pressure at the upstream stagnation point and p_∞ is the free stream static pressure. Figure 10(b) shows the stagnation pressure coefficient as a function of the Hartmann number. It displays a monotonic decrease with increasing Ha and approaches a constant value slightly smaller than 1 as Ha grows. In the flow around a cylinder the stagnation pressure coefficient is expected to be 1 according to the inviscid Bernoulli equation. In practice, however, at low Reynolds numbers it deviates from this value [24].

V. CONCLUSIONS

Most of the studies of flows under nonuniform magnetic fields have been devoted to duct flows with a field that varies in the streamwise direction, as approximately occurs at the entrance or exit of the poles of a magnet. Instead, the present contribution offers a theoretical treatment of a different problem: the flow past strongly localized magnetic fields. The

main objective of the work is to stress the possibility of generating vorticity in creeping flows under localized fields. This may be of importance in applications where mixing or heat transfer enhancement is needed. But this problem can also shed new light on flows in ordinary hydrodynamics [10], as in the analysis of hydrodynamic effects of localized forces, which is of importance in flows produced by self-propelled bodies [16,17]. We have analyzed the interaction of a uniform two-dimensional creeping flow with a localized magnetic field produced by a dipolar distribution. First, an approximated magnetic point dipole was considered and analytic solutions were found using a perturbation expansion in the small Reynolds number that is valid only for small Hartmann numbers. Since the magnetic point dipole presents a singularity at the origin, the analytic solutions diverge at this point but present the correct behavior as the distance from the dipole tends to infinity. These solutions show in a simple manner how the Lorentz force created by the interaction of the induced electric currents with the dipolar field acts as an obstacle for the flow and generates vorticity. The interaction of the uniform flow with a finite magnetic dipolar distribution was explored numerically for $\mathrm{Re}=0.05$, using a finite difference method in the range of Hartmann numbers $1 \leqslant \mathrm{Ha} \leqslant 100$. Different flow regimes were observed according to the value of the Hartmann number. In fact, the analysis of the induced electric current paths allows an explanation of the different flow patterns. For small Ha, the flow is only slightly deviated from its oncoming direction, while an increase in its value creates stagnation zones or steady vortical structures. It is remarkable that the creeping flow past a localized magnetic field presents many similarities with the flow past bluff bodies, particularly for Hartmann numbers smaller than 50. For instance, when $\mathrm{Ha}=30$, a pair of counter-rotating vortices appears inside the magnetic obstacle zone. But important differences arise when the Hartmann number reaches values higher than 50. In fact, a new pair of counter-rotating vortices appears in the central region of the magnetic obstacle, expelling the other pair to the exterior zone. This effect appears to be related not only to the strength of the applied field, but also to the finite area of the magnetic obstacle. Evidently, this kind of vortical structures has no analogies with the flow past bluff bodies.

ACKNOWLEDGMENTS

Support from UC MEXUS-CONACYT and DGAPA-UNAM under Project No. IN111705-2 is gratefully acknowledged.

[1] M. Abdou *et al.*, Fusion Eng. Des. **54**, 181 (2001).
[2] L. Bühler, J. Fluid Mech. **326**, 125 (1996).
[3] B. Mück, C. Günther, U. Müller, and L. Bühler, J. Fluid Mech. **418**, 265 (2000).
[4] Y. Kolesnikov and A. Tsinober, Magnetohydrodynamics (N.Y.) **3**, 300 (1972).
[5] M. Frank, L. Barleon, and U. Müller, Phys. Fluids **113**, 2287 (2001).
[6] J. Sommeria and R. Moreau, J. Fluid Mech. **118**, 507 (1982).
[7] K. Messadek and R. Moreau, J. Fluid Mech. **456**, 137 (2002).
[8] A. Alpher, H. Hurwitz, R. H. Johnson, and D. R. White, Rev. Mod. Phys. **32**, 758 (1960).
[9] T. Alboussière, J. Fluid Mech. **521**, 125 (2004).
[10] O. Andreev, Yu. Kolesnikov, and A. Thess, Phys. Fluids **18**, 065108 (2006).
[11] A. E. Hansen, D. Marteau, and P. Tabeling, Phys. Rev. E **58**, 7261 (1998).
[12] H. Salas, S. Cuevas, and E. Ramos, Magnetohydrodynamics **37**, 38 (2001).
[13] H. Honji, J. Phys. Soc. Jpn. **60**, 1161 (1991).
[14] H. Honji and Y. Haraguchi, J. Phys. Soc. Jpn. **64**, 2274 (1995).
[15] Y. D. Afanasyev and V. N. Korabel, J. Fluid Mech. **553**, 119 (2006).
[16] Y. D. Afanasyev, Phys. Fluids **16**, 3235 (2004).
[17] Y. D. Afanasyev and V. N. Korabel, Phys. Fluids **16**, 3850 (2004).
[18] S. Cuevas, S. Smolentsev, and M. Abdou, J. Fluid Mech. **553**, 227 (2006).
[19] R. H. Good and T. J. Nelson, *The Classical Electromagnetic Field* (Wiley, New York, 1971).
[20] M. McCaig, *Permanent Magnets in Theory and Practice* (Wiley, New York, 1977).
[21] M. Griebel, T. Dornseifer, and T. Neunhoeffer, *Numerical Simulation in Fluid Dynamics* (SIAM, Philadelphia, 1998).
[22] H. M. Blackburn and R. D. Henderson, J. Fluid Mech. **385**, 255 (1999).
[23] C. K. H. Williamson, Annu. Rev. Fluid Mech. **28**, 477 (1996).
[24] M. M. Zdrakovich, *Flow Around Circular Cylinders. Vol. 1: Fundamentals* (Oxford University Press, Oxford, 1997).